Mapping distribution of fractures in a reservoir with P-S converted waves

By ELIAS ATA and REINALDO J. MICHELENA
Intevep, SA
Caracas, Venezuela

Where reservoir rock is very impermeable (limestones, cherts, dolomite, etc.), fractures may provide all or most of its porosity and effective permeability. Studies of producing oil wells in fractured limestones have determined a single fracture of width 1 mm, under favorable reservoir conditions, can provide sufficient permeability to yield over 1500 m^3 (240 bbl) of oil per day. Consequently, mapping locations of high intensity fractures and determining their orientation/lateral extent could be of great value in reservoir development, especially for locating horizontal well sites.

Multicomponent surveys (nine components) have proven effective in delineating fracture strike, density, and lateral extent. However, high acquisition and processing costs, limited availability of S-wave sources, and volume/quality of S-waves rendered such surveys unpopular. P-S converted waves were deemed a cost-effective alternative and were investigated in the 1980s. The reasons were simple. P-S converted waves are (1) generated with a compressional source, (2) less labor intensive, (3) expected to contain the same information as S-waves, and (4) more practical in 3-D surveys (reduced data volume and cost). In practice, however, dealing with P-S waves is more cumbersome than with nonconverted waves.

Through careful survey design/acquisition/processing, anisotropy parameters can be successfully estimated from P-S converted waves. Here, we present results from a well controlled P-S converted wave survey to estimate anisotropy parameters in a fractured reservoir in southwest Venezuela.

Folding and faulting in the area resulted from the collision of the Caribbean Plate with the South American Plate in the Middle-Eocene. The present stress regime in the area results from the orogeny of the Andes which are situated about 50 km west. Note from Figure 15 that most faults terminate at or before the top horizon, which implies that no major folding or faulting resulted from the Andes orogeny. However, this later event may be responsible for reactivation of some of the faults and realignment of open fractures along its maximum axis.

The objective of the survey was to determine the best locations and trajectories for drilling horizontal wells. We discuss acquisition, processing, and analyses related to this data set. Finally, we generate anisotropy maps (fracture orientation and density) within the reservoir and correlate results with available well data.

Background. S-wave birefringence or splitting refers to an incident wave which, after encountering an azimuthally anisotropic layer, becomes two waves that travel at two different velocities. The amount of splitting or anisotropy is the time lag and/or relative amplitude differences between the two waves. The faster wave, with polarization parallel to fracture strike, propagates at the velocity of the unfractured rock; it is called S,. The slower wave, with polarization perpendicular to the strike, propagates at the velocity of the fractured rock; it is known as S,. Similarly, S-waves produced by P-wave conversion at an azimuthally anisotropic interface, immediately undergo the same phenomenon.

Traveltime differences between S_1 and S_2 are a low resolution measure of anisotropy, while their relative amplitude differences are a high resolution measure of local anisotropy within a fractured layer. In fact, amplitude variations may be the only diagnostic of highly fractured rocks in relatively thin layers and where data have limited resolution. Therefore, extreme care must be taken in dealing with multicomponent data to insure that final S_1 and S_2 sections possess balanced energy and that relative true amplitudes are preserved. Conditions for balanced amplitudes must be achieved during acquisition via source/receiver consistencies and line orientation with respect to fracture strike.

A full multicomponent survey consists of three sources (P-wave, inline, and crossline) and three receivers (vertical, radial and transverse) which yield nine unique observations. By contrast, in a *P-S* survey, we need only one P-wave source and three component receivers to yield three unique observations. Such components are illustrated in Table 1 as a function of source-receiver polarization.

Table 1.
Multicomponent survey

Source \ Receiver	x	y	z
X	Xx SV-SV	Xy SV-SH	Xz SV-P
Y	Yx SH-SH	Yy SH-SV	Yz SH-P
Z	Zx P-SV	Zy P-SH	Zz P-P

Consider a seismic line, a P-wave source (equivalent to an inline polarized source upon conversion to an S-wave), and three-component receivers over an isotropic and homogeneous medium. The *P-S* energy will be observed on the inline receivers having the same polarization as the converted S-wave energy. On the transverse receivers, energy should be minute to null and independent of the orientation of the seismic line.

If the above experiment is repeated over an azimuthally anisotropic and homogeneous medium (Figure l), the

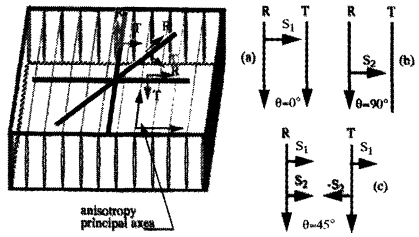

Figure 1. Expected P-S energy on radial (R) or inline and transverse (T) or crossline receivers when a seismic line is (a) parallel, (b) perpendicular, and (c) at an angle to fracture strike.

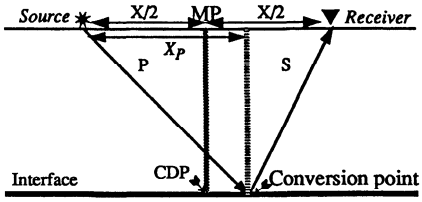

Figure 2. Geometry of a conversion point with respect to the midpoint (MP) between source and receiver for nonconverted waves. While MP is at an equal distance X/2 between the source and the receiver, the conversion point is at a distance Xp with respect to the source location, with Xp > X/2.

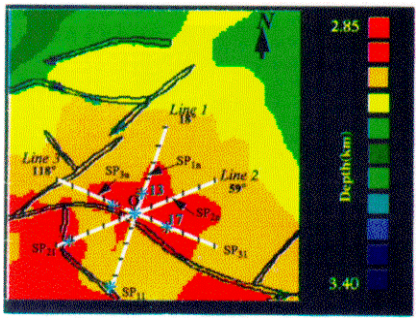

Figure 3. Multicomponent seismic lines superimposed on structural contour map of the fractured producing formation. 0 is the point of intersection, * denotes a well location, and SP, shotpoint location ($_i$ = line, $_j$ = shotpoint).

expected P-S energy on the horizontal receivers can be generalized as follows:

1) Line is *parallel* to strike. Energy travels at the faster velocity of the unfractured medium and is mainly observed on the inline component; little to no energy should be observed on the transverse component (Figure 1 a).

2) Line is *perpendicular* to strike. This time the wave propagates at the slower velocity of the fractured medium and, again, little to no energy should be observed on the transverse component (Figure lb).

3) Line forms an *angle* with strike. This is the general case. Both S_1 and S_2 will be observed on each of the two horizontal components. Amplitudes will be scaled by $\cos^2 0$ and $sin^2\theta$ on the radial receivers and $sin\theta cos\theta$ and $-sin\theta cos\theta$ on the transverse receivers (Figure lc).

In full multicomponent surveys, and in all three cases, S_1 and S_2 modes can be fully recovered by recording once with an inline source and then with a crossline source. The main difference is that in cases l-2 (assuming uniformly fractured media), data are acquired along principal axes of symmetry and energy rotation is not needed. But, in case 3, energy rotation is needed so that sources and receivers are along the principal axes of symmetry. Thus, relative traveltime and amplitude variations between S_1 and S_2 can be related directly to anisotropy effects.

In a *P-S* survey, cases 1 and 2 suggest unfavorable conditions for anisotropy analyses since only one wave type can be observed. Moreover, it is impossible for alternative polarizations of the P-wave source to generate both modes from the same spatial locations. Also, recording two orthogonal lines with one source type (inline or crossline) is not equivalent to recording a single line with both inline and crossline sources. Consequently, case 3 (ideally 45") is favorable in *P-S* surveys since both S_1 and S_2 may be recovered, with balanced energy, through rotation analyses (only receiver rotation is possible) from a single line. With angles much different from 45" (especially where data are poor), amplitude differences may be misleading in detecting local anisotropic effects. Therefore, if fracture strike is not known, a fan of seismic lines would be required with the hope that a near 45° line with respect to fracture strike may be attained.

In the subsurface, the conversion point (Figure 2) varies as a function of horizontal offset, depth, and ratio of P-wave velocity to S-wave velocity. As a consequence, common conversion point (CCP) gathers for multiplicity stacking must account for such phenomena in processing converted waves. Failure to do so can yield improperly focused and mispositioned converted wave events. Prestack migration and asymptotic approximation of a CCP are two alternatives for processing *P-S* converted waves. Here, we used the asymptotic approximation due to the simple structure of the area.

Survey design and acquisition. Three 10-km multicomponent lines (due to unknown fracture strike) were centered over the areas of interest, with an intersection point coinciding with a well location. Each line also intersected at least two additional wells with the most relatively complete logs. Depth contour maps from existing P-wave data show two systems of normal faults: one runs northeast-southwest and the other northwest-southeast. The azimuths of two lines were almost parallel to the fault systems; the third line almost bisected them and formed an angle of approximately 40" with line 1 (Figure 3).

A noise-spread test examined the quality of converted waves, severity of ambient noise, surface wave dispersion, and optimum source-receiver spacing. Other tests determined that a charge of 1 kg at a depth of 10 m gave good S/N ratio and significantly attenuated surface waves.

The subsequent survey was designed, based on analysis of the noise test, to enhance the quality of *P-S* waves. Acquisition parameters are given in Table 2. Implementation (possibly the most crucial stage in multicomponent surveys) required extensive effort to maintain consistent receiver coupling, leveling, and orientation. Finally, each uphole time and charge depth were recorded for later use in static corrections and near-surface modeling.

Diagnostic of azimuthal anisotropy from raw data. The importance of data quality in anisotropy analysis cannot be overemphasized. Raw shot records were examined for traveltime, amplitudes, and events with respect to location and azimuth of each line. Figure 4 is a true amplitude plot of raw shot gathers of radial and transverse components from two locations along each line. All records exhibit high data quality with minimum noise contamination (mainly from oil pumps). No significant *P-S* energy can be observed on the transverse components of the three lines above the

Table 2. Survey parameters

GEOMETRY	
Number of traces/component	216
Total number of 3-C receivers	648
Near offset trace	17m(-55ft)
Far-off set trace	3672 m(- 12 000 ft)
Number of elements per string	6
Separation of geophone elements	3.4 m (- 11 ft)
Total geophone spread	10km (-33000ft)
Total number of shotpoints per line	124
Shotpoint space intervals	51 m (- 167 ft)
Charge depth	10m (-33ft)
Source offset	17m (-55 ft)
Charge size	1 kg (- 2.2 lb)
Geophone pattern: 6 elements centered around the flag over 17 m (- 55 ft)	
RECORDING	
Total number of traces	648
Sample interval	2 ms
Low cut	out
High cut	128 Hz
Notch filter	out
Record length	6s

first strong event around 3.1 s, which implies the interval above this reflector is relatively isotropic.

In Figure 4a, lines 1 and 3 show strong energy on both components but energy appears only on the radial component of line 2a. The lack of energy on the transverse component of this line could mean (1) the media is relatively isotropic at this locality or (2) the line is close to one of the principal axes of symmetry (i.e., parallel or perpendicular to the fractures). Energy remains nonexistent-to-weak on line 2's transverse component until the shotpoint approaches the reservoir (Figure 4b, middle) when it starts to gradually increase. In contrast, the energy on line 1 's transverse component decreases in similar fashion but never vanishes. Energy on line 3's transverse component increases slightly in a northwest direction. Close examination of the normal

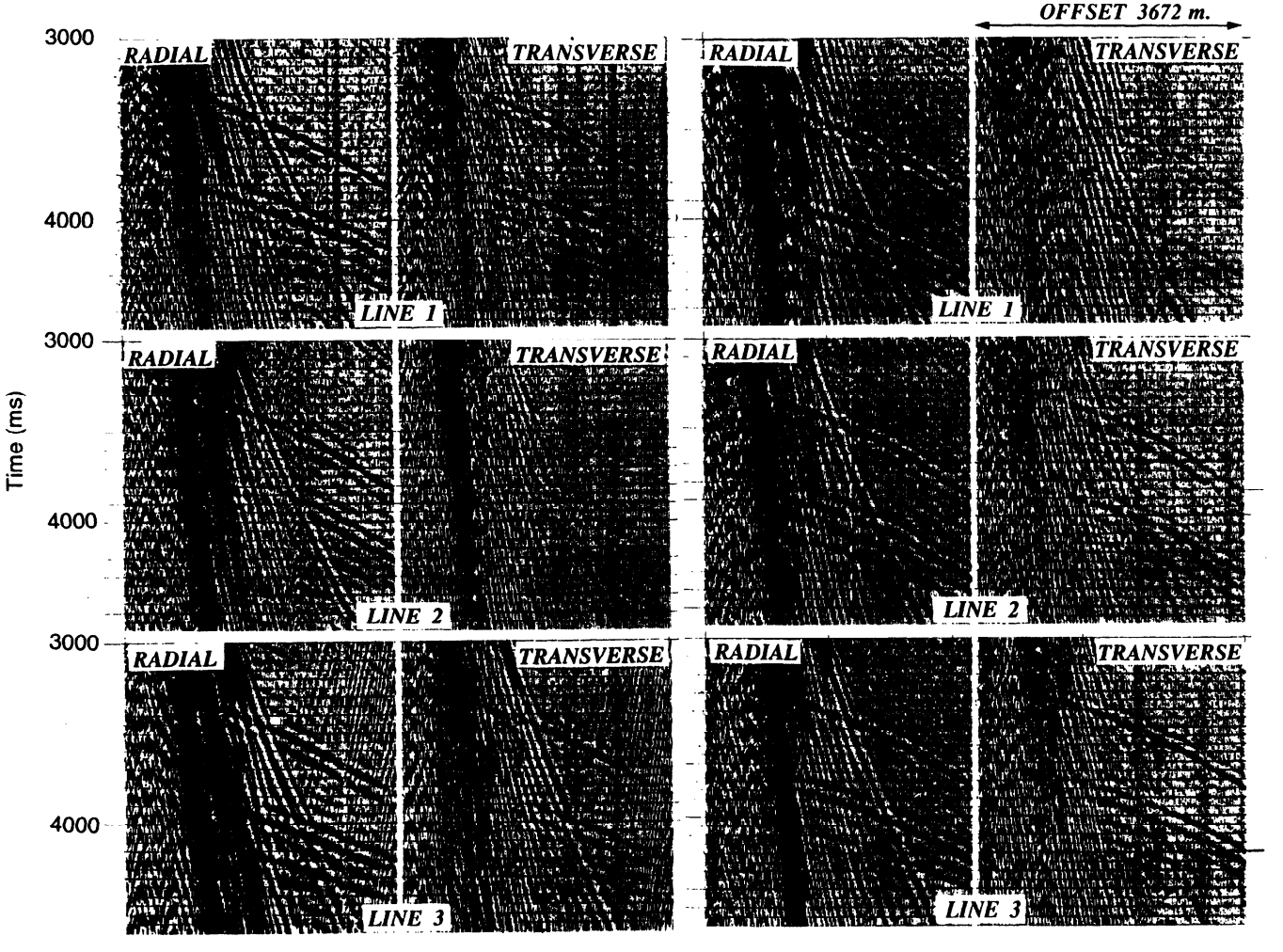

Figure 4. Raw shot records of the radial and transverse from shotpoints located at (a) start and (b) middle of each line. These panels,are representative of the overall data quality of the survey.

Table 3. Vertical and horizontal components processing sequence

VERTICAL
Geometry and field statics
Bad trace edit
Surface waves attenuation
CDP sort
Brute stack
Deconvolution
Statics and velocity iterations
Geometric spreading
NMO and statics corrections
Stack
Q-compensation
Migration
***P-S* (HORIZONTAL)**
Geometry and field statics
Bad trace edit
Surface waves attenuation
CDP sort
Brute stack
Calculate V_p/V_s ratio (from traveltimes on *P* and *P-S* brute stacks)
Modify CDP geometry to accommodate conversion point geometry
CCP sort
Statics and velocity iterations
Geometric spreading
NMO corrections
Stack
Rotation analyses (determine angles)
Restart with CCP sorts
Apply rotation angles to CCP gathers and get S_1 and S_2 gathers
Repeat statics and velocity iterations on S_1 and S_2 gathers
Apply NMO and statics corrections
Q-compensation
Migration
Anisotropy analyses

moveout between radial and transverse components of the same shotpoint (e.g., top of Figure 4a and bottom of Figure 4b) shows that receivers pointing roughly south-north (radial component on line 1 and transverse component on line 3) have a larger moveout than those pointing west-east. This indicates fracture strike in a west-east direction.

Relative changes of *P-S* energy on the transverse components of the three lines can be explained by many fracture patterns, some of which are illustrated in Figure 5. Model A comprises a fracture system that strikes almost perpendicular to line 2 (at SP_{21}) and rotates about 30° to the northeast where line 1 becomes almost perpendicular to it. The angular relations between each of the lines with respect to the fracture system are defined as: (1) line 1 with $\theta_{11} < \theta_{1n}$, (2) line 2 with $\theta_{21} > \theta_{2n}$, and (3) line 3 with $\theta_{31} < \theta_{3n}$. Under these conditions, *P-S* energy on a multicomponent receiver spread, progressing from SP_{il} to SP_{in} (i=1–3) should yield similar energy splitting as observed on the field records of Figure 4.

In model B, fracture strike is parallel to the lower half of line 2 and rotates to become parallel to line 1 in the north. This model yields similar responses to model A, the only difference being rotation of the principal axes of anisotropy by 90°. Another plausible system is model C which comprises two fracture systems consistent with the fault planes in the area. Later analyses and well data show that model C is more representative of the subsurface. Based on the theory that open fractures tend to align along the direction of maximum regional stress and, consequently, that perpendicular fractures may be closed, the fracture system of interest may run southeast-northwest.

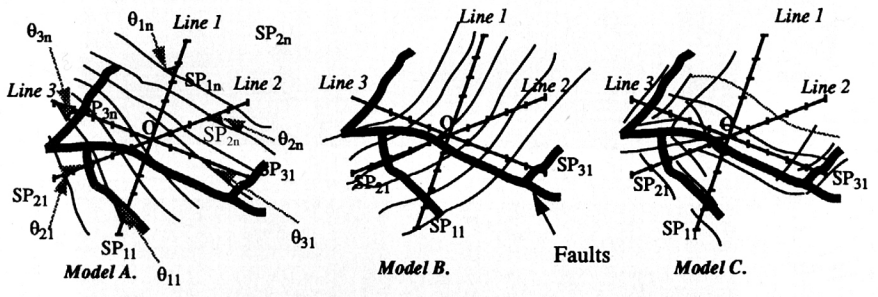

Figure 5. Possible fracture patterns that may yield the energy variations exhibited by the shot records. θ_{ij} is the angle between the seismic line and fracture strike; i indicates line number and j shotpoint location with respect to start and end of the line.

Data processing. The processing scheme was designed to preserve relative true amplitude, maximize the frequency band, and optimize the velocity and statics solutions for all components. A typical processing flow of *P-S* converted wave data is shown in Table 3. The data were processed to a brute stack to estimate V_p/V_s from the *P* and *P-S* traveltimes down to the target zone. If lateral and vertical velocity variations or overburden anisotropy are significant, the processing sequence may have to be repeated for different V_p/V_s ratios with the asymptotic gathering approach. However, for our data, an average V_p/V_s ratio of 2.5 yielded well focused *P-S* sections above and below the target zone.

The migrated stack sections of all components are shown in Figure 6. All display good quality with reflections that could be easily correlated among the different components (see events 1-4). Energy variations on radial and transverse components (Figure 6a,b) are consistent with raw shot records.

To evaluate processing parameters, all like components of all migrated sections were checked at the intersection point and against synthetic seismograms (where available). Figure 7 shows the *P*-wave sections of lines 1 and 3 tied with synthetic seismograms generated with sonic logs from wells that intersect these lines. Similarly, Figure 8 shows the three *P*-wave sections tied with each other at their intersection point (O). The good tie between synthetic and *P*-wave sections at the well location indicates good quality processing. Moreover, the consistency of the processing among all lines is supported by the good tie among the three lines.

Comparison of traveltimes, at the intersection point, of the *P-S* sections for the radial component of all lines is shown in Figure 9. The mis-tie of the *P-S* data is to be expected due to the interference of the S_1 and S_2 modes which are recorded on the same component. However, after rotation a good tie must be produced between each mode of each pair of the three lines.

Rotation analysis. This step determines the angle that aligns observed data with the principal axes of symmetry. Figure 10 is a schematic illustration of four and two component rotation. Where full elastic wave data are available, rotation (source and receiver)

analysis using four components (Xx, Xy, Yx, and Yy, as shown in Table I) allow for better constraints in determining the correct rotation angle. In this case, the validity of the rotation angle can be checked with residual energy on the off-diagonal components (i.e., energy is minimized on the Xy and Yx components, Figure 10b).

By contrast, for *P-S* converted waves, only two components (Figure 10c) are available to perform rotation analysis (only receivers can be rotated). Consequently, rotation angles cannot be checked directly and therefore may be less reliable than those derived from four-component rotation. Crosscorrela-Tion and energy ratio between S_1 and S_2 (Figure 10d) have been suggested as diagnostics to check the validity of the rotation angle. The assumption behind the former is that a symmetric wavelet can be obtained only when both components are perfectly separated. The second approach assumes that the energy ratio of a specific event attains a maximum when the correct angle is reached (i.e., the seismic line is parallel to fracture strike). The second approach is effective where 3-D *P-S* converted wave data are available and various azimuths efficiently sampled.

Another approach is to apply a rotation angle and evaluate the traveltime differences between S_1 and S_2. An angle that maximizes traveltime differences between the two sections can be considered correct. After application of the rotation angles, a second attempt at tying the three lines yielded the results shown in Figure I I. A good tie is produced among the three lines between 3200-4100 ms. The wavelet stretch on the S_2 component (above 3500 ms) is inherent only in the data of line 3. The good tie after the application of a single rotation angle and the lack of energy on the transverse component (Figure 4) can signify that overburden anisotropy effects are negligible.

Figure 12 is a map view of the rotation angles obtained from the three lines using energy ratio as criterion to validity. These angles are plotted with respect to north for each group of CDPs that corresponds to the same angle. Angles between lines have been interpolated and results are more reliable along and in the neighborhood of the three lines. Fracture orientations tend to run subparallel to the fault systems that cut the reservoir. Model C in Figure 5. that was predicted from unprocessed records, is in good agreement with the results in Figure 12.

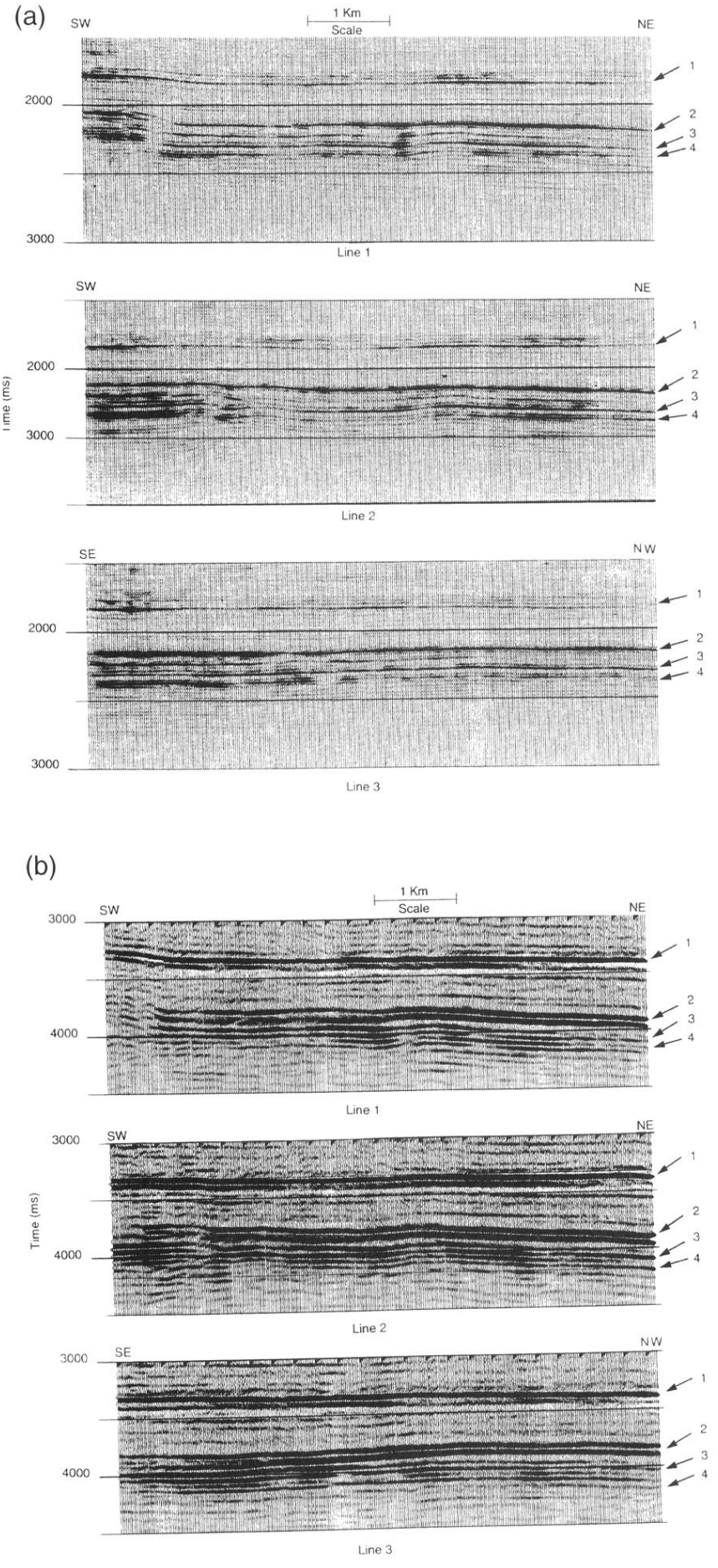

Anisotropy analysis: traveltimes. Traveltime variations were compared between S_2 and S_1 sections (after rotation) over various locations and along each of the three lines. Figure l3a shows the tic between both modes at about 2 km from the start of each line. A sizable mis-tie that varies with depth (between 8-14 ms) is observed on line I; line 2 shows a good tie overall; and line 3 shows a mis-tie on the order of 6 ms below 4000 ms. In Figure 13b the traces are tied against each other at the intersection point of the three lines (compare with Figure 11, also note persistent wavelet stretch on line 3). At this location, sizable mis-ties appear on lines 1 and 3. Mis-tie is smaller on line *2*. Finally, in Figure 13c, the two modes are compared at a distance of 7 km from the start of each line. Traveltime differences continue to vary vertically and horizontally, ranging in values from a few ms to 20+ ms. As both horizontal components had the same acquisition and processing parameters, variations between the modes may only be attributed to anisotropy.

Anisotropy analysis: amplitudes. Reflection amplitude anomalies between corresponding horizons on both sections have been used as a high resolution indicator of local anisotropy (i.e., an intensely fractured zone is implied when S_2 has lower amplitudes than S, or discontinuities not equal to S,). Figure *14* shows a 500 ms window, of both S, and S_2 modes, for a section of line I. Although SIN ratio is relatively higher in the S_2 section due to line orientation with respect to fracture strike (60-70°), regions of relatively lower amplitudes on S_2 can he compared directly with corresponding locations on S,. Time picks from S_2 traces (Figure 14 bottom) were superimposed over S, traces (Figure 14 top). Traveltime differences tend to increase with depth and amplitude anomalies correlate in general with larger traveltime differences. Highlighted areas arc obvious anomalies that can be detected visually. Mapping these traveltime and amplitude variations permits better representation of spatial anisotropy distribution.

Anisotropy maps. To better visualize traveltime variations along the three lines. anisotropy maps were constructed as follows:

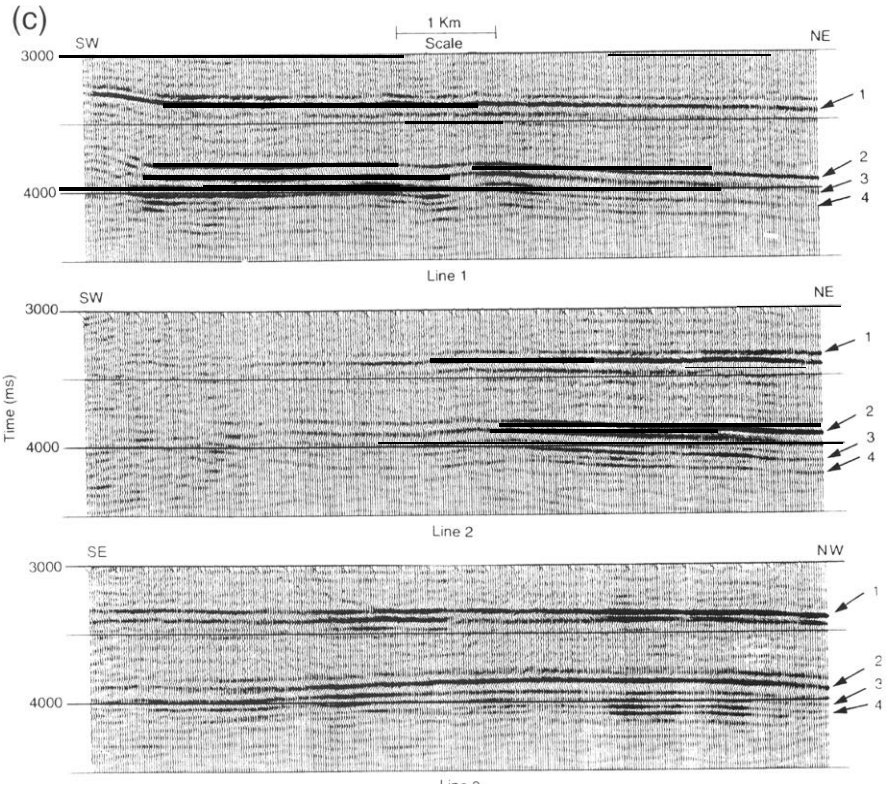

Figure 6. Relative true amplitude plots of migrated stack sections of the three lines: (a) vertical component, (b) radial, and (c) transverse. Events of interest are identified l-4.

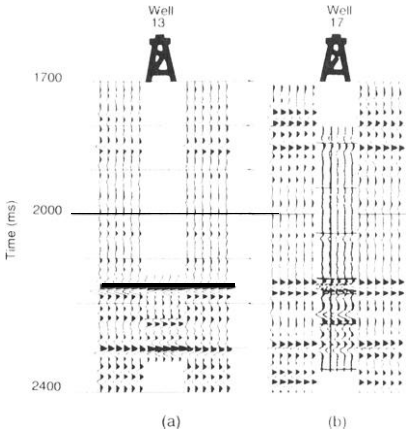

Figure 7. Tying P-wave sections of lines 1 and 3 to synthetic seismograms generated from sonic logs of wells 13 (a) and 17 (b).

1) Events over converted wave sections were correlated with *P-wave events*.

2) Horizons of interest were time picked (l-4 in Figure 6).

3) Traveltime differences of S_2 and S, were computed between corresponding depth points of each horizon.

4) Traveltime differences were plotted for fist horizon versus depth point coordinates over all depth points for all lines.

5) Traveltime differences were removed (time shift S_2 to align with S, at each CDP) from first horizon and steps 3-4 repeated for the remaining horizons.

(If the differences in step 4 were positive, fracture strike in northwest-southeast direction was implied. Negative values implied that strike has rotated to southwest-northeast.)

The traveltime difference map for the base of the zone of interest is shown in Figure 15. The margin of error for the time picker is ±2 ms. Values on the order of -4 (light blue) and +12 ms (yellow) are consistent with the data. Lower and higher values are the result of missing data and/or numerical interpolation. The blue-shaded region inside the heavy zero contour line implies that the faster mode in this area is in the southwest-northeast direction. All other colors indicate a fracture strike roughly in the direction of line 3 (northwest-southeast). The negative traveltime differences are smaller than the positive ones, which implies the northwest-southeast orientation induces relatively higher

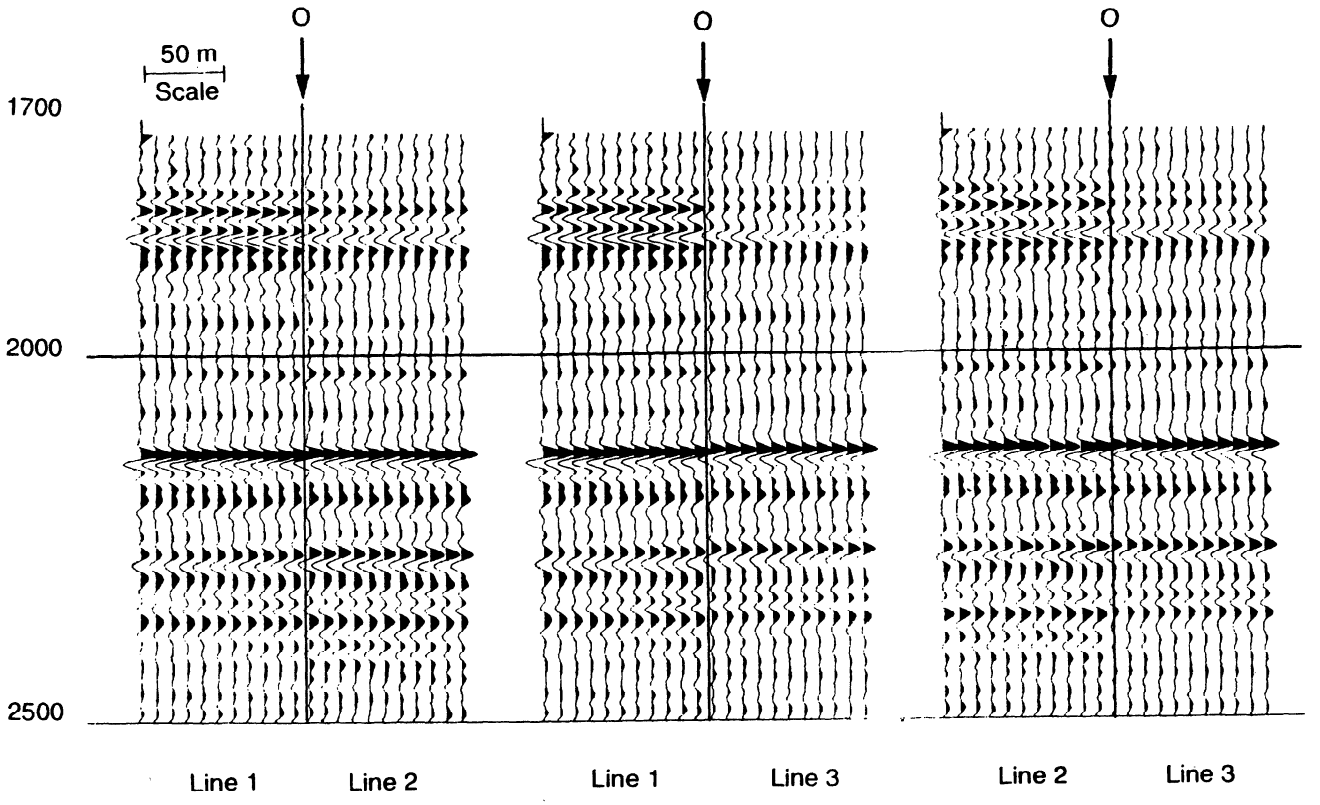

Figure 8. Tying P-wave sections at intersection point (0). There is good agreement between the lines over all depths with respect to traveltimes.

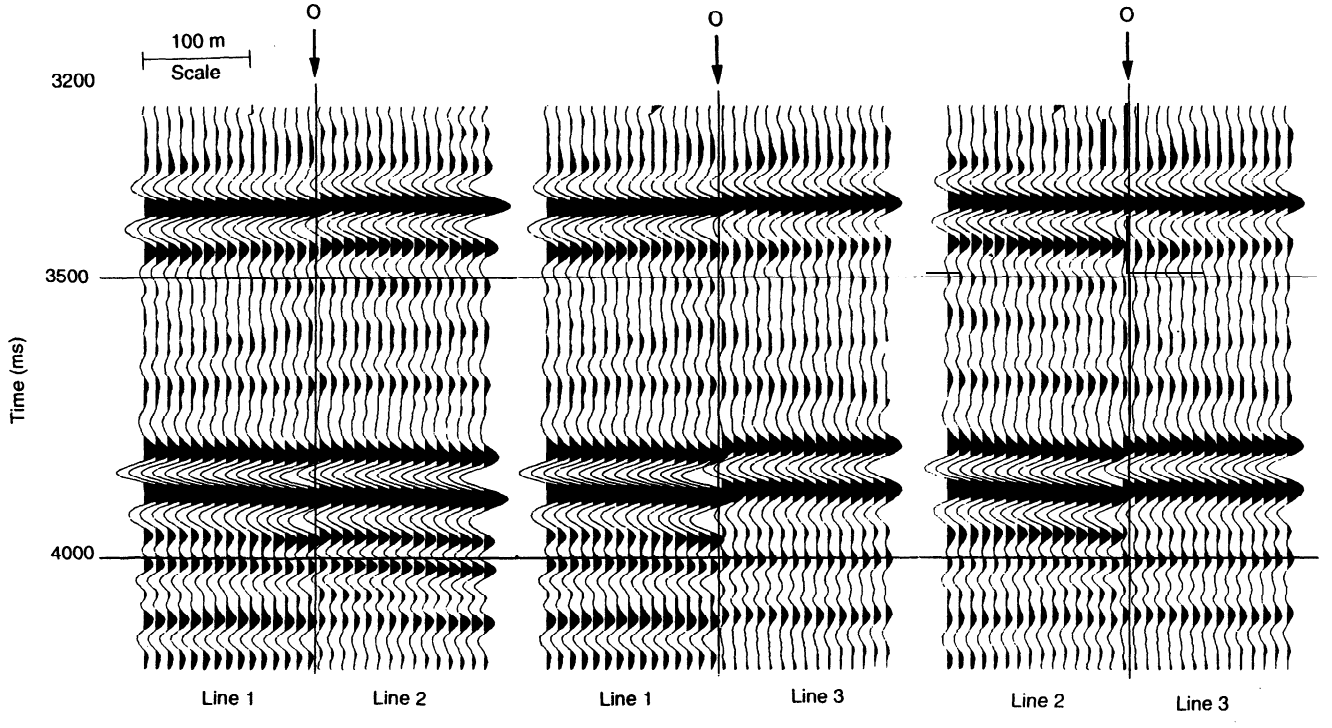

Figure 9. Tying P-S sections of the radial component at the intersection point before rotation. Compare with the P-wave tie of Figure 7.

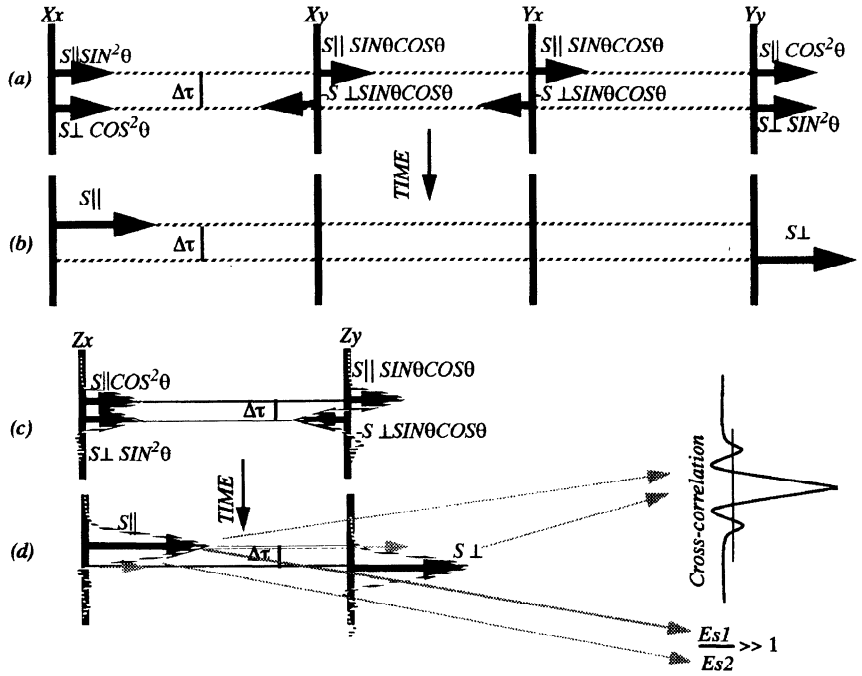

Figure 10. Reflection events from a multicomponent survey over azimuthally anisotropic media: (a) four-component before rotation; (b) four-component rotated; (c) two-component before rotation (converted waves); and (d) two-component rotated. Capital letter designates a source. Small letter designates receiver polarization. The two null components corresponding to Xy and Yx are missing in the case of P-S data. Also, the P-S waves yield a $\Delta\tau$ that is, in general, half of that obtained from S-S data. Cross-correlation of S_1 and S_2 yields a symmetric wavelet and the energy ratio Es1/Es2 reaches a maximum when the correct rotation angle has been encountered and applied to the data. (After the correct rotation, shaded vectors must reduce to zero.)

anisotropy than the southwest-northeast orientation.

These results are consistent with images from FMS logs and wellbore ellipticity analyses, where two fracture systems can be observed as shown in the rose diagram in the upper right corner of Figure 15. The more dominant system strikes northwest-southeast and is prominent in all analyzed wells; the other system appears in fewer wells. Borehole ellipticity analyses and published material ("The world stress map project," *Journal of Geophysical Research*, 1992) indicate the direction of the present maximum regional stress is roughly parallel to line 3. Since open fractures tend in general to align with the direction of the maximum regional stress, fractures striking in this direction appear a more favorable target for horizontal drilling than their orthogonal counterparts.

The high resolution P-wave data show that faults on various scales traverse line 1, which is roughly orthogonal to line 3 (Figure 15). Figure 16 shows a 300 ms window over 5 km sections of both lines (from SP, to about the intersection point). Some of the many faults that can be traced along both lines have been identified with the red dotted lines. Comparison of the number of faults that cross both lines

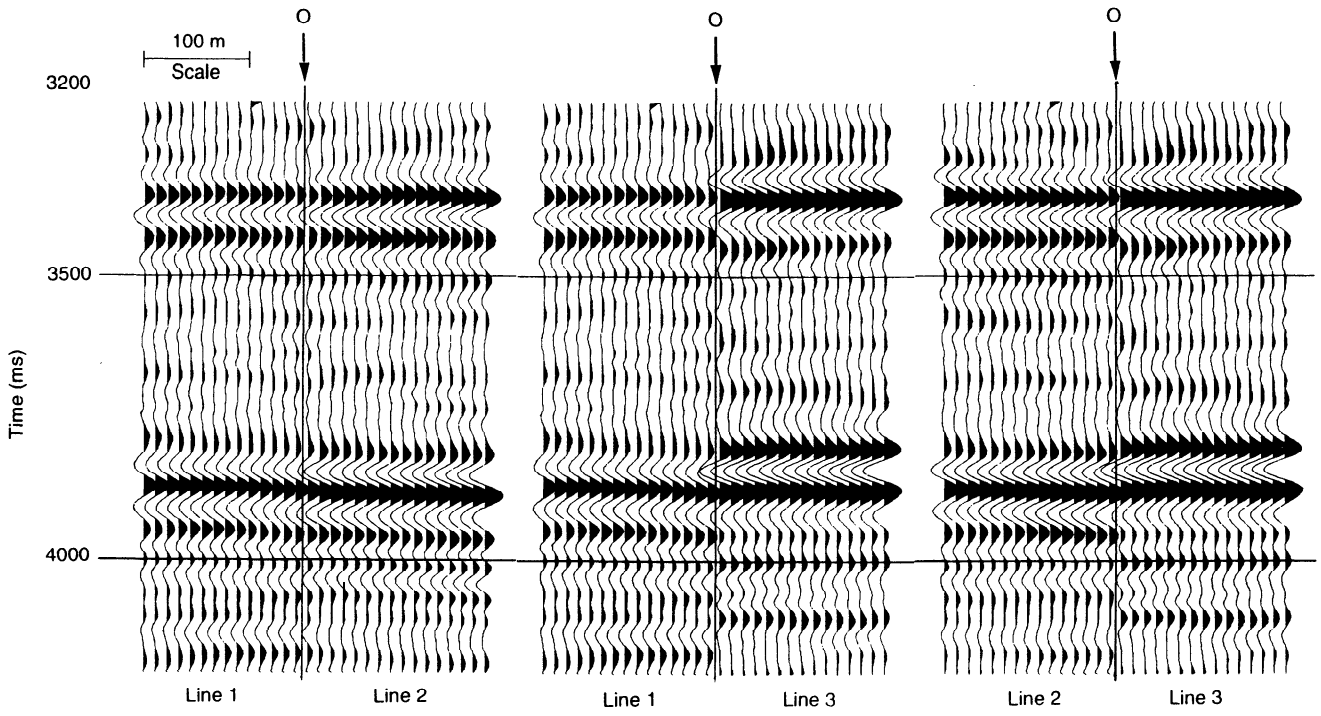

Figure 11. Tying S_1 and S_2 components at intersection point after application of rotation angles (compare with Figure 9).

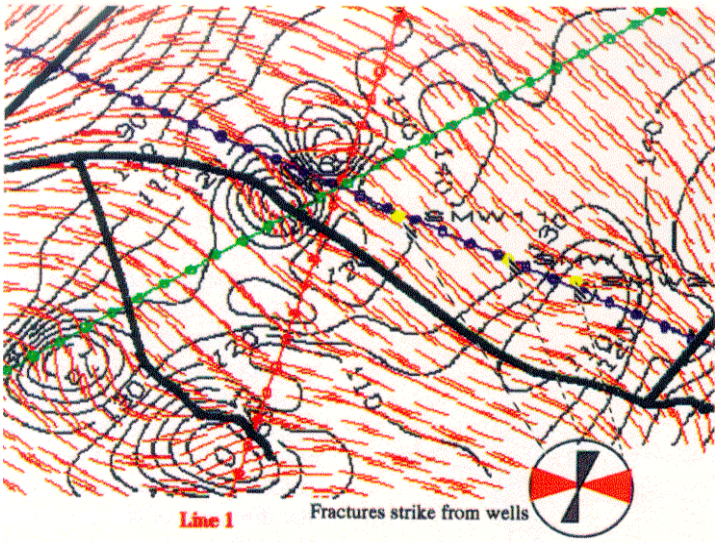

Figure 12. Map view of fracture orientations at horizon 3 (Figure 5), obtained from rotation analyses of the three lines. The orientation is, in general, subparallel to line 3, more in the southeast than the northwest portion of the line. Note agreement between model C (Figure 5) and fracture orientation.

establishes that the major fault system is parallel or subparallel to line 3 (i.e., orthogonal to line 1). A 3-D P-wave survey that has been acquired will allow accurate mapping of the faults with which the fracture patterns may be associated. In the mean time, if we're to associate fractures with the abundance of faults that can be traced across line 1, it would be logical to say that the fractures in this area strike in the general direction of line 3.

A pilot horizontal well was located and drilled in the blue colored area in Figure 15 (red segment above line 3). The location appears logical given a well defined fracture system and based on sparse well data. However, the well yields less than 50% of projected daily production and its orientation is parallel to that of the maximum regional stress in the area. Zones where traveltime and amplitude variations overlap are considered likely candidates for horizontal well locations. Reorientations of upcoming horizontal wells, such that their trajectories intercept the fracture strike at a near-orthogonal direction, can improve oil recovery.

Discussion. The ability of multicomponent data, especially P-S converted waves, to provide azimuthal anisotropic parameters is determined primarily by the quality of the data acquired. If S-wave birefringence cannot be observed in field data, chances are the survey will not meet its objectives. The clear anisotropy effects displayed by the data in this paper can be attributed to careful design and implementation of the survey. Consistent receiver orientation, leveling and coupling together with controlled source depth and energy level design minimize extraneous traveltime and amplitude variations in the data that may be confused with azimuthal anisotropic effects. A real acquisition advantage of P-S converted wave surveys is that data quality can be improved significantly where explosive sources are deployed below the weathering layer.

Rotation analysis of P-S converted waves is more cumbersome than 4-component rotation as shown in Figure 11. For reliable use of amplitudes as a high resolution measure of local azimuthal anisotropy (fracture intensity), final rotated S_1 and S_2 sections from P-S converted waves should have balanced amplitudes. This situation must be accounted for during the survey design by laying the seismic line to cross the fracture strike at an angle of approximately 45 degrees. If the fracture strike is not known, a fan of 2-D lines must be recorded to increase the probability of crossing fractures at -45 degrees. In a 3-D, P-S survey this problem can be solved by having good azimuthal coverage that allows more reliable mapping of fractures orientation and area1 variations of highly fractured zones. In the 3-D case, rotation angles can be evaluated reliably by comparing energy along different azimuths of various orthogonal lines.

P-S converted wave data must be carefully processed to account for their asymmetric travelpath and preserve true amplitude information. Normally, P-S converted waves are gathered using a constant VP/VS ratio (averaged at the target zone) which yields focused images in the vicinity of the target horizon. Such an approach is sufficient in simple geologic structures and where vertical and lateral velocities vary smoothly. However, in the presence of complex structures and/or strong velocity variations, prestack migration or dip moveout processing are more effective approaches to process P-S converted waves. The structural simplicity of our experimental area allowed the gathering of the data with a constant Vp/Vs, ratio averaged from the surface to the target horizon, which is confirmed by the ease of correlation between the P-P and P-S reflection events.

The P-S converted wave data collected in this survey exhibit significant azimuthal anisotropy in the form of traveltime and amplitude differences, on the S_1 and S_2 components. Furthermore, the principal axes of symmetry vary as a function of location and azimuth along the seismic lines. The P-wave sections tie fairly well at the intersection point of the three lines, while the *P-S* lines exhibit a sizable mis-tie that varies vertically and laterally. These azimuthal anisotropic effects appear to be caused by two fracture systems associated with two fault systems in the area of the experiment.

The dominant system is closely aligned with the direction of maximum regional stress. A second system, orthogonal to the first, appears on the maps as well as on well data.

Traveltime and amplitude anomalies indicate possible locations for positioning and orienting horizontal wells. A previously drilled horizontal well, parallel to the direction of maximum horizontal stress, did not yield expected results. The fracture system that appears to dominate borehole and surface data. strikes northwest-southeast. Amplitude anomaly maps, reinterpretation of the fault patterns from 3-D data, and additional well information (VSP, dual sonic logs, etc.) may further refine these results. Finally, elastic modeling of the fracture patterns (Figure 5) may further explain the observed results.

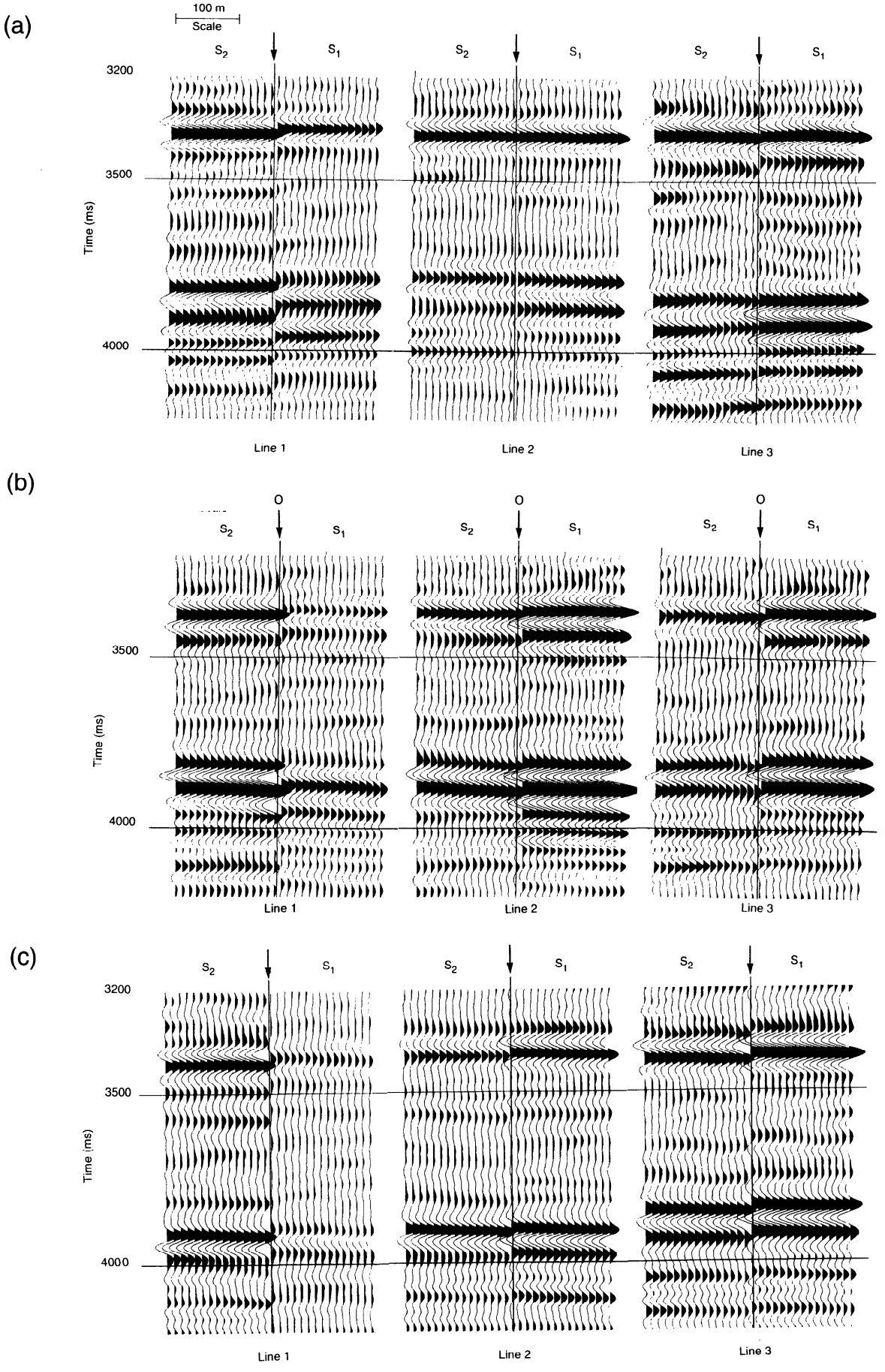

Figure 13. (a) Tying S_1 and S_2 components 2.5 km from start of each line. (b) Tie is 5 km (intersection point) and (c) tie is 7 km from start of each line.

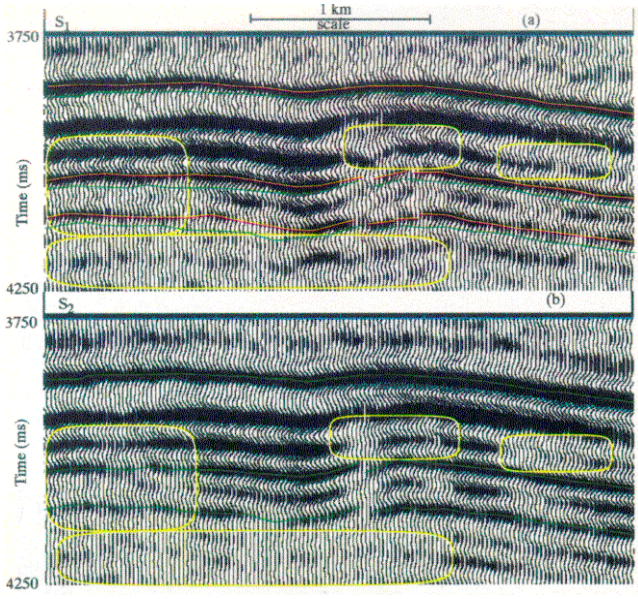

Figure 14. Relative amplitude plots of S_1 and S_2 of line 1 over the reservoir. Green and red lines represent time picks from corresponding horizons on the S_2 and S_1 sections, respectively. Yellow boxes indicate zones of amplitude differences. And, separation between red and green lines in S_1 plot represents traveltime differences between both modes. Note that S_2 has higher S/N ratio than S,; amplitudes appear equal due to angle dependent scaling applied in rotation.

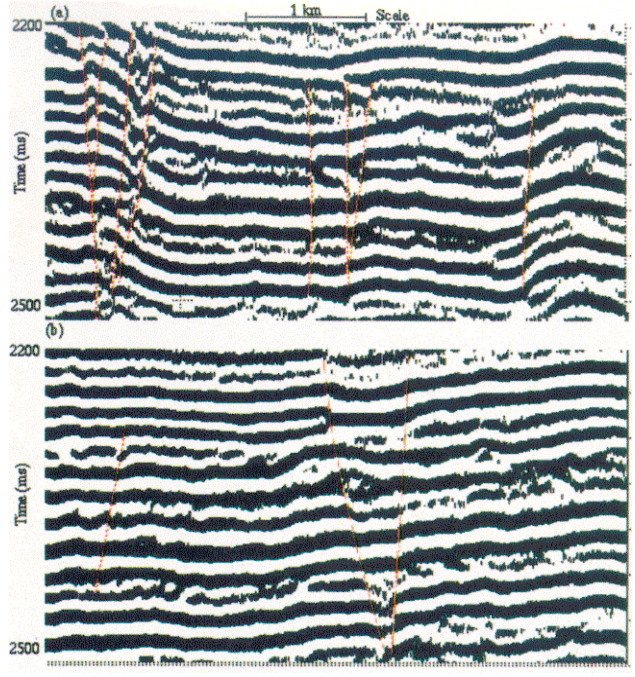

Figure 16.300 ms window over reservoir from (a) line 1 and (b) line 2. High resolution allows fault patterns shown in Figure 2 to be redefined. Obvious faults are approximated with dotted red lines; additional local faults can be identified and associated with the fracture pattern in the area (correlate with faults that cross line 1 in Figure 2).

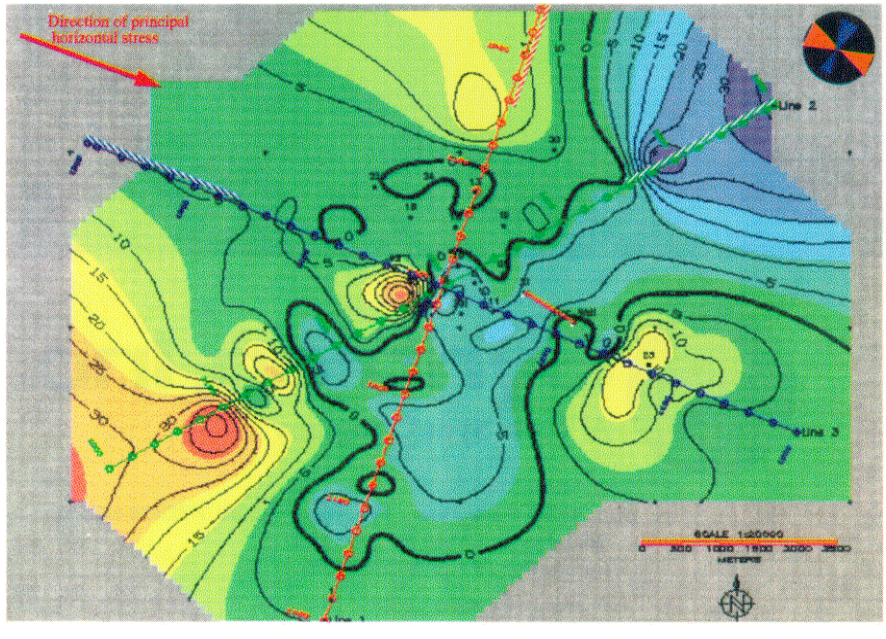

Figure 15. Anisotropy map at the base of the reservoir. Red segment above line 3 (blue) indicates location and orientation of the horizontal well. Traveltime differences are identified by their corresponding values on each contour line. Data points that fall at the ends (marked with dotted lines), or in between the seismic lines, are numerically interpolated. The numbers and corresponding black dots indicate vertical well locations. The rose diagram at the upper right corner indicates fracture orientation obtained from borehole data.

Acknowledgments. We wish to thank Corpoven, SA and Intevep, SA for their support and permission to publish these results. We thank Jim Gaiser; Sven Treitel, and Robert Greaves for their editing and helpful suggestions to improve this manuscript. Also we thank Robert Reilingerfor providing the reference to the World Stress Map Project. Finally, we are indebted to our colleagues Manuel Gonzalez, Jesus Sierra, Javier Perez, Jose M. Salazar and Elias Andara for their assistance in all phases of this work.

Elias Z. Ata received a BS in computer technology (1980) from the University of Houston and an a MS in geophysics (1991) from the University of Texas-Dallas. He did acquisition work with various seismic contractors from 1980 to I983 and joined ARCO in 1984 where he specialized in acquisition and processing of multicomponent data. He joined Intevep in 1992 to initiate multicomponent projects for anisotropy studies in fractured reservoirs. He is a member of SEG and SOVG.

Reinaldo Michelena received a BS in physics (1984) from Universidad Simon Bolivar. He researched electrical methods for Intevep from 1985 to 1988. With the aid of an Intevep scholarship, he received an MS (1990) and PhD (1993) in geophysics from Stanford University. He worked on both the Seismic Tomography Project and the Stanford Exploration Project. He is now conducting research in multicomponent seismic, anisotropy, borehole seismic methods, and nonlinear inverse problems. He is a member of SEG and SOVG.